The Analysis of the Small-Signal AC-Response of Bovine Enamel Membranes

H. P. F. Scholberg, J. M. P. M. Borggreven, F. C. M. Driessens

Dental School, University of Nijmegen, P.O. Box 9101, 6500 HB Nijmegen, The Netherlands

J. Schoonman

Laboratory of Inorganic and Physical Chemistry, Delft University of Technology, P.O. Box 5045, 2600 GA Delft, The Netherlands

Biophysical Chemistry / Dental Enamel / Diffusion / Electrical Properties

The ion permeability of bovine enamel membranes can be estimated from impedance spectroscopy. In this study the 6-parameter model, a previously proposed operational description of the frequency dependence of the impedance of an enamel membrane is compared with a model which uses a Constant-Phase-Angle (CPA) element, and which is proposed as an onset to a more mechanistic description of enamel impedance spectra. The model using the CPA element is shown to be a valid description for the measured impedance data. The parameter values for R_0 and ω_{max} (the angular measuring-frequency where the imaginary part of the membrane-impedance is maximal) obtained using this model, confirm that these parameters can be employed as predictors for bovine enamel permeability.

Introduction

A key-feature of enamel structure is the parallel-arrangement of densely packed crystallites, long hexagonal rods with a diameter of approximately 0.01 μm and a length of approximately 0.1 μm. They consist of a mineral which resembles the very slightly soluble hydroxyl-apatite. Bundles of these crystallites together constitute the prismata, keyhole shaped interlocking structures, 1.5 μm diameter and 50 μm length, oriented nearly perpendicular to the tooth-surface in a way to offer both ruggedness and a certain amount of flexibility, necessary to prevent breakage of the tooth enamel. In the body of a prisma a highly ordered parallel arrangement of the crystallites is found. At the contact-regions between adjacent prismata some of the parallel orientation of the crystallites is lost. This explains the occurrence of an inter-prismatic phase, consisting of narrow regions with a more random orientation of the crystallites, where the spaces between them will approach (as may be inferred from SEM-pictures) the dimensions of the crystallites themselves. In these relatively open regions the enamel mineral becomes vulnerable to physiological attacks. One of them, the acid attack that results from metabolic activity in the plaque (a sticky layer of bacteria and organic debris that may cover the enamel cap), may cause caries. At this point the relevance of enamel permeability enters: it determines the ease with which agressive substances may invade the enamel. In case of an acid attack the permeability controls the speed of penetration of the acids into the enamel and hence the progress of subsurface demineralisation, which causes the lesions that are characteristic for the caries process. Thus the rate of progress of the caries process was demonstrated to be approximately proportional to the square root of bovine enamel permeability [1].

Enamel permeability can be measured chemically as the rate of diffusion of ions through an enamel membrane [2]. In previous works [3, 4], the impedance of bovine enamel membranes, for which the permeability for small ions was known from radiotracer studies [2], was analysed. In order to find parameters, which can be used as predictors for enamel permeability, a 6-parameter model was proposed as a phenomenological description of the "skewed-arc" impedance spectrum of bovine enamel (see Fig. 1a). Using this approach, R_0 (the width of the arc) and ν_{max} (the frequency at the top of the arc) were demonstrated to be predictors of bovine enamel permeability. In the present study the above mentioned 6-parameter model is compared with the analysis

Ber. Bunsenges. Phys. Chem. *91*, 129–134 (1987)
0005–9021/87/0202–0129 $ 02.50/0

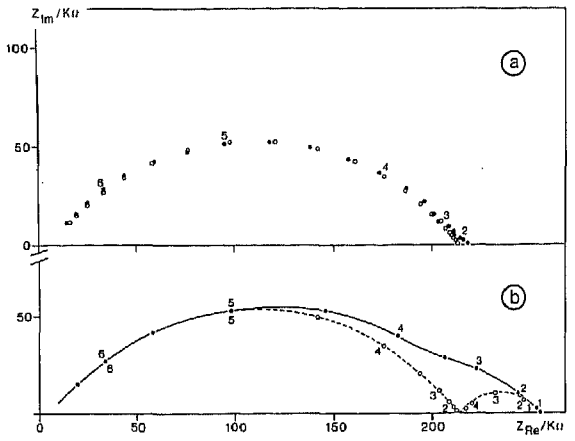

Fig. 1
a) Typical Cole-Cole plot of a complex impedance measurement for a tooth enamel membrane: solid dots indicate the measuring points, open dots indicate the "fit" obtained using the "backward" method, numbers along the curve give $\log(\omega)$, where: ω (the angular frequency) $= 2\pi\nu$ (the measuring frequency).
b) Simulated Cole-Cole plot that would point to the presence of a surface-film: the solid curve indicates the overall impedance-spectrum, the left semicircle, denoted with the dotted line and open dots, refers to the spectrum of the bulk-membrane ($\log(\omega_{max,mem}) = 4.8$), the right semicircle refers to the spectrum of the surface-film ($\log(\omega_{max,film}) = 2.8$), numbers along the curve give $\log(\omega)$.

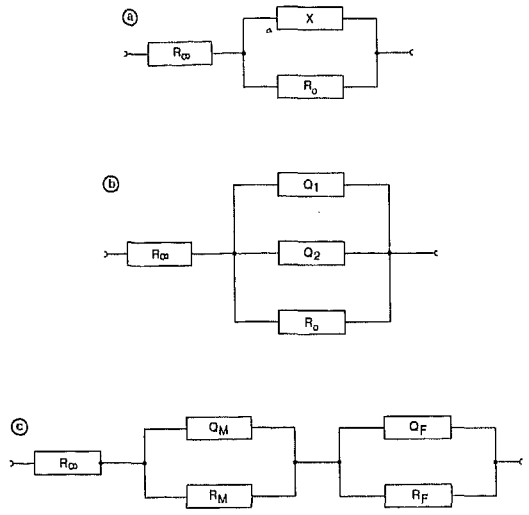

Fig. 2
a) Equivalent circuit used in analysing enamel membrane impedance spectra: -X-indicates a complex circuit element, which has to be characterised.
b) Electric analogue that corresponds with the distribution of Fig. 6a (Q denotes a CPA-element).
c) Equivalent circuit that corresponds with the distribution of Fig. 6b: R_M and Q_M add up to the RQP-branch of the membrane, R_F and Q_F add up to the RQP-branch of the surface-film.

of the small-signal AC response of enamel membranes, using an equivalent circuit comprising resistive elements, and a Constant-Phase-Angle element with an admittance of the form:

$$Y^* = K_\alpha x(i\omega)^\alpha \quad (0 \leq \alpha \leq 1)\,. \tag{1}$$

This model, which can be thought of as a basis for a mechanistic description of the small-signal AC response of enamel is henceforth referred to as "the CPA-model".

Materials and Methods

Models Used for the Analysis of Impedance Spectra of Enamel Membranes

The 6-Parameter Model

For a description of this model the reader is referred to the equivalent circuit of Fig. 2a. The symbols used in this figure have the following meaning:

R_0: the "width" of the arc on the Z_{Re}-axis.
R_∞: the "offset" on the Z_{Re}-axis for measuring frequencies (ν) $\to \infty$. R_∞ comprises the resistance of the electrolyte solution, the electrodes and the residual membrane resistance (if any).
$-X-$: Enamel-Diffusion-Impedance (EDI) element.

For the complex admittance, $Y^* = Y_{Re} + iY_{Im}$, of the EDI element, the form:

$$Y^* = A\omega^n + iB\omega^m \tag{2}$$

was obtained from a least-squares analysis of conductance-frequency and susceptance-frequency data [4]. The Kramers-Kronig (KK) relations (see [5]), however, require $n = m$, and the following relation between A and B to hold:

$$B = A \cdot \tan(n\pi/2)\,. \tag{3}$$

Raistrick, Ho, and Huggins [6, 7] have introduced the admittance form (2) to fit impedance data on fluorites and silicates. It should, however, be emphasized [8], that the use of (2) with A and B, and n and m taken independent may introduce unwarranted degrees of freedom in fitting equivalent circuits to experimental admittance/impedance spectra. In many instances, the small-signal AC response of bovine tooth enamel membranes revealed $n \neq m$, thus rendering form (2) to polar coordinates impossible. This ambiguity is not met in CPA-model.

The CPA-Model

In the CPA-model the element $-X-$ in the equivalent circuit of Fig. 2a is replaced by a Constant-Phase-Angle element with an admittance which reads in polar form:

$$Y^* = K_\alpha x(i\omega)^\alpha \quad (0 \leq \alpha \leq 1)\,. \tag{4}$$

This element has been employed in many studies for fitting response data on solid ionic conductors and semiconductors. Expanding (4) in cartesian coordinates, it follows that:

$$Y^* = K_\alpha \omega^\alpha [\cos(\alpha\pi/2) + i \cdot \sin(\alpha\pi/2)]\,. \tag{5}$$

Macdonald and Brachman [9] have shown the real and imaginary parts in (2,4) to be properly related by the K-K relations. For $\alpha = 0$ form (4) represents a conductance, for $\alpha = 1$ form (4) represents the admittance of a capacitance, and for $\alpha = 0.5$ it models classical Warburg diffusion. Other values for α are commonly related to non-uniform diffusion processes [10]. With regard to the 6-parameter model, the CPA-model fully accounts for existing interrelations between A and B, and n and m. Hence, the equivalent circuit in Fig. 2a with the CPA-element for $-X-$ is reduced to a 4-parameter model.

Methods Used for the Analysis of Impedance Spectra of Enamel Membranes

The following methods could be used to determine the parameter values of an electric analogue for an electrochemical system:

The "Direct" Method (Complex Non-Linear Least-Squares Analysis)

In complex (where complex refers to the simultaneous fitting of real and imaginary data to an equivalent circuit) non-linear least-squares analysis the model or equivalent circuit used to describe the impedance (Z) or admittance (Y) spectrum of the system can be represented [11] by the complex function:

$$f^*(\omega,\chi) = f_{\mathrm{Re}}(\omega,\chi) + \mathrm{i}\cdot f_{\mathrm{Im}}(\omega,\chi)\,. \tag{6}$$

In (6) ω denotes the angular frequency ($\omega = 2\pi\nu$) and χ is a vector of model parameters. Complex Z (or Y) measurements of the form: $\mathrm{Re}_j + i\cdot \mathrm{Im}_j$, done in a range of angular frequencies $\omega_j (j = 1$ to $N)$, are analysed by searching the value of χ which minimises the (weighted) sum of squared differences S_{SQ}:

$$S_{\mathrm{SQ}} = \sum_j \{W_j^{\mathrm{Re}}\cdot[\mathrm{Re}_j - f_{\mathrm{Re}}(\omega_j,\chi)]^2 + W_j^{\mathrm{Im}}\cdot[\mathrm{Im}_j - f_{\mathrm{Im}}(\omega_j,\chi)]^2\}. \tag{7}$$

Here W_j^{Re} and W_j^{Im} are weights, associated with measurement j.

In a previous study [4] this problem was solved using the IMSL® routine ZXS_{SQ}, a finite difference variant of the Levenberg-Marquardt algorithm [12, 13], assuming the above mentioned weight factors to be unity. Macdonald et al. [11], using the same approach, propose as weights the reciprocal variances of the measurements.

The analysis of complex Z and Y data used by Tsai and Whitmore [14], incorporates the suggestions of Sheppard, Jordan, and Grant [15, 16] who describe an integral adaptation of the Marquardt algorithm itself to "fitting" complex Z or Y data. In a forthcoming study the results obtained using this "integral approach" will be presented.

The ambiguity encountered in relating complexity and connectivity of the chosen model to the "goodness-of-fit" obtained when using it, cannot always be resolved, since there may be no physical (or statistical) rationales for using a more complex model, despite the fact that such a model may result in a better "fit". There is no a priori knowledge concerning the model to be used in analysing enamel membrane impedance spectra, so the experimental data in this study were provisionally investigated, using what may be referred to as:

The "Backward" Method (Semi-Graphical Resolution of Multi-Component Impedance Diagrams)

When there is some a priori knowledge concerning the nature and conductivity of all but a few of the elements that will add up to a physically satisfactory model-description for experimental data, the "backward" method can be used to analyse the behaviour of the remaining elements [14, 17]. Starting from the general circuit that is given in Fig. 2a, the frequency-dependent behaviour of element $-\mathrm{X}-$ is investigated in detail. In this procedure the following steps can be distinguished. Estimates for R_0 and R_∞ are calculated from the Cole-Cole plot (see Fig. 1a) by extrapolation to $\omega = 0$ and $\omega = \infty$ respectively. Then the estimated value of R_∞ is substracted from the measured Z_{Re}-values. Subsequently the resulting $(Z_{\mathrm{Re}} - Z_{\mathrm{Im}})$ pairs are converted in $(Y_{\mathrm{Re}} - Y_{\mathrm{Im}})$ pairs. Finally $1/R_0$ is subtracted from the Y_{Re}-values.

In case the CPA-model is valid, and the correct values for R_0 and R_∞ are taken (see below), two parallel lines will result in a $\log(Y)$ versus $\log(\omega)$ plot (see Fig. 3). According to Eq. (5) the slopes of both lines will be α, whereas the resulting offsets for Y_{Re} *and* Y_{Im} will be respectively:

$$\log[K_\alpha \cos(\alpha\pi/2)] \text{ and } \log[K_\alpha \sin(\alpha\pi/2)]\,. \tag{8}$$

From these equations K_α can be calculated.

Errors in the estimates of R_0 and R_∞ will only slightly influence the $\log(Y)$ versus $\log(\omega)$ curves when looking at the mid-range of measuring frequencies ($3 \leq \log(\omega) \leq 5$), where the CPA-element dominates the impedance behaviour. However, characteristic deviations will occur in the $\log(Y_{\mathrm{Re}})$ versus $\log(\omega)$ curve at low frequencies ($\log(\omega) \leq 3$) when the estimated R_0 is in error (see Fig. 4a). Given an incorrect estimation of R_∞, departures from ideal behaviour will arise in both curves (see Fig. 4b) at high frequencies ($\log(\omega) \leq 5$). The correctness of the resulting values for R_0, R_∞, K_α and α can be checked by calculating from them the $(Z_{\mathrm{Re}} - Z_{\mathrm{Im}})$ pairs for the range of measuring frequencies used, and by subsequently comparing them with the measured values (this last step is of course an intrinsic part of the "fitting" procedure described in: "The 'direct' method" (Methods and materials)).

Simultaneous Measurement of Radio-Tracer Diffusion and Electrochemical parameters

To compare the electrochemical measurements with the results obtained in diffusion experiments, the following procedure was used (described in more detail by Borggreven et al. [2] and Scholberg et al. [3, 4]). Slices of bovine enamel (thickness 0.200 mm) were mounted as membranes between the two compartments of diffusion cells. Both compartments were filled with 15 ml of an aqueous solution containing 2 mmol/l Hepes (N-2-hydroxyethylpiperazine-N'-2-ethanesulfonic acid) buffer of pH 7.4, 10 mmol/l RbCl, glycerol and sorbitol. Moreover 40 µmol/l chlorhexidine-HCl (Hibitane®) was added to prevent bacterial growth. To one compartment [^{3}H]-sorbitol, [^{14}C]-glycerol, $^{36}Cl^-$ and $^{36}Rb^+$ were added as radiotracers, while equivalent amounts of non-radioactive material were added to the other compartment to equalise the overall concentration of the diffusing species on both sides of the membrane. Transport through the enamel was monitored by sampling the tracers in the non-labelled compartment. The liquid-scintillation counting of radio-isotopes and the calculation procedures necessary to obtain the diffusion coefficients for Rb^+ (D_{Rb}) and Cl^- (D_{Cl}) are described by Borggreven et al. [2]. From the resulting diffusion-coefficients

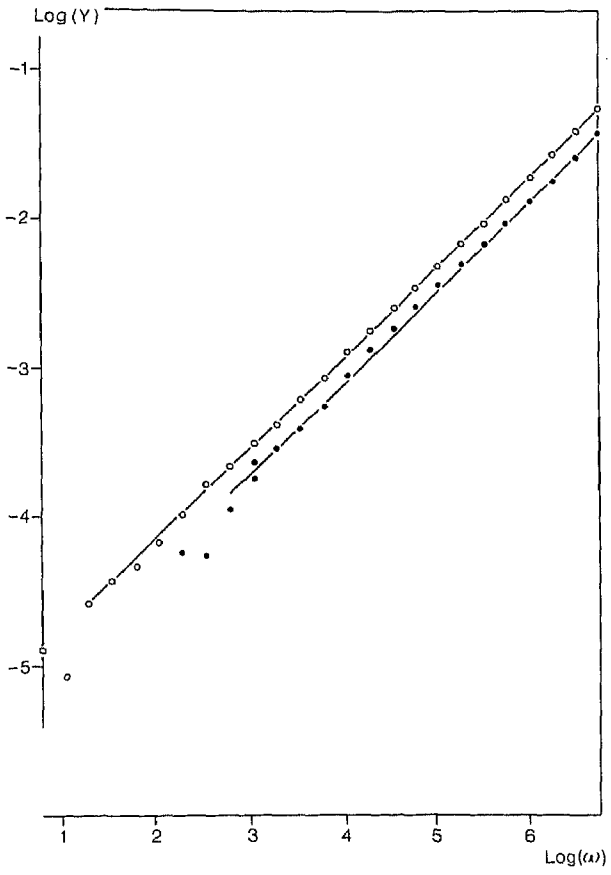

Fig. 3
$\log(Y)$ versus $\log(\omega)$-plot for the spectrum of Fig. 1a: solid dots indicate $\log(Y_{\mathrm{Re}})$-values, open dots denote $\log(Y_{\mathrm{Im}})$-values. The lines indicate the results of linear regression analysis (since the Y_{Im}-curve lies above the Y_{Re}-curve, it follows that $\alpha > 0.5$)

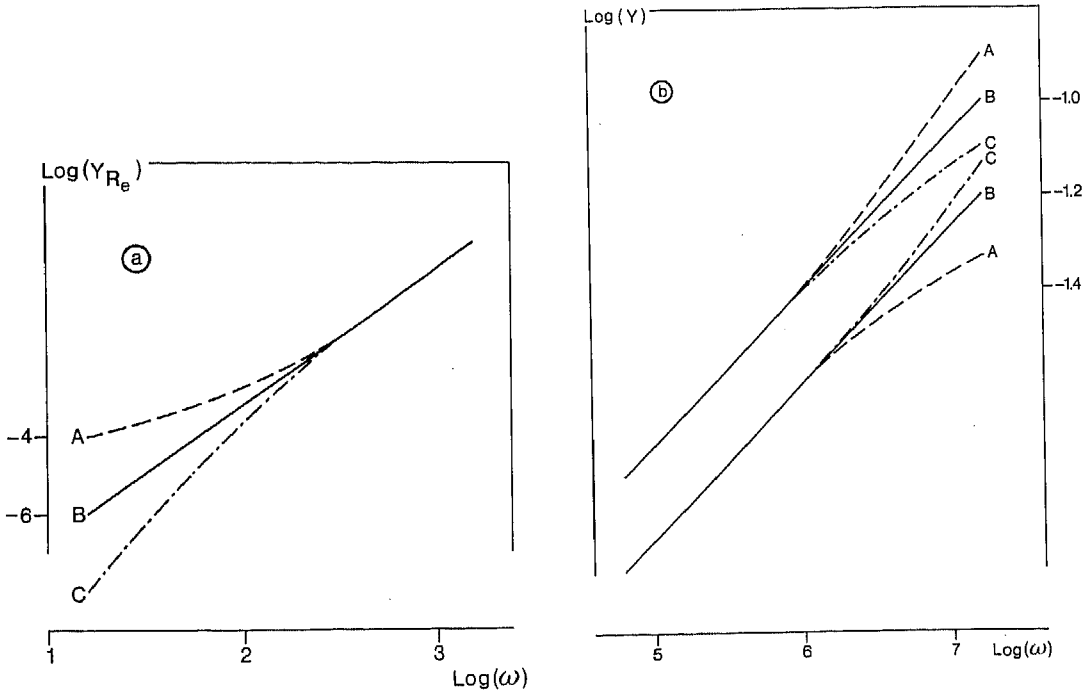

Fig. 4
a) Influence of erroneous estimates of R_0 on $\log(Y_{Re})$ versus $\log(\omega)$-plots. (A): R_0 too large; (B): R_0 correct; (C): R_0 too small.
b) Influence of errors in the estimated value of R_∞ on $\log(Y)$ versus $\log(\omega)$-plots (upper trace Y_{Im}, lower trace Y_{Re}): (A): R_∞ too large; (B); R_∞ correct; (C): R_∞ too small.

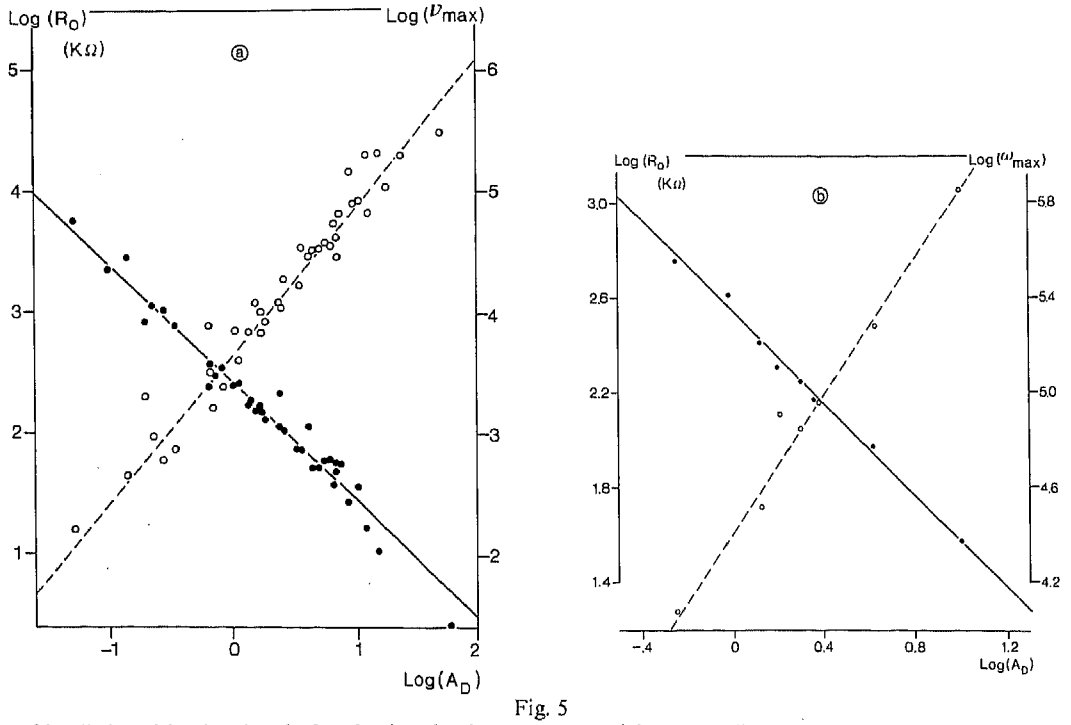

Fig. 5
a) Suitability of $\log(R_0)$ and $\log(\nu_{max})$, calculated using the 6-parameter model, as a predictor of enamel permeability: measuring points plus results of weighted linear regression analysis.
b) Suitability of $\log(R_0)$ and $\log(\omega_{max})$, calculated using the CPA-model as a predictor of enamel permeability: measuring points plus results of linear regression calculations.

a membrane's value of A_D (the charge-corrected diffusion-coefficient) was calculated as follows:

$$A_D = (2D_{Rb}\,D_{Cl})/(D_{Rb} + D_{Cl})\,. \qquad (9)$$

Several times during the sampling period (14 days) the impedance spectra of the membranes were recorded by placing calomel-electrodes (Radiometer K401) in either compartment of the diffusion-cell and measuring Z_{Re} and Z_{Im} (the real and imaginary part of the membrane impedance) at discrete intervals in the frequency range 1 Hz to 1 MHz [4]. To prevent contamination of the electrodes with radio-isotopes and cross-contamination between parallel experiments, the electrodes were equipped with disposable salt bridges, made from micro-pipette tips (Eppendorf blue, 1000 µl)

filled with agar KCl. From these spectra each membrane's value of R_0 and ω_0 (the angular frequency where Z_{Im} is maximal) were calculated. For the calculation of $\omega_{\max}$ the following expression was derived:

$$\omega_{\max} = (R_0 \cdot K_\alpha)^{1/\alpha}. \tag{10}$$

Here α is the power that governs the frequency dependence of the CPA-element and K_α is its premultiplier (cf. section: "The CPA-model").

Results

The 6-Parameter Model

This model was tested by analysing 64 enamel membranes [4]. In that study $\nu_{\max}$ (the frequency where Z_{Im} is maximal) and R_0 were found to be good predictors for A_D, the charge-corrected ionic permeability of the enamel (see Fig. 5a). To compare Fig. 5a with the results obtained by using the CPA-model (section Results), please note that $\omega_{\max}$, the parameter used in this study, equals $2\pi\nu_{\max}$.

The CPA-Model

In order to evaluate the CPA-model, 8 membranes were analysed using this model description. Using the "backward" method of analysis, the correlation coefficients for the $\log(Y_{\text{Re}})$ versus $\log(\omega)$ plots ranged from 0.997 to 0.999. For the imaginary part a range of 0.9990 to 0.9998 was obtained. Comparing the measured Z-values with the values generated from R_0, R_∞, K_α and α as obtained via the "backward" method, generally speaking a good "fit" was found (see Fig. 1a), whereas in individual cases a low-frequency ($\log(\omega) < 3$) deviation may be noticed. (In those cases relatively high values for Z_{Re} were measured, revealing a Cole-Cole plot resembling the solid line of Fig. 1b, but with less pronounced deviation from the semi-circle). The suitability of R_0 and $\omega_{\max}$, both calculated from this model, as predictors for enamel permeability, can be read from Fig. 5b. When performing linear regression analysis according to the model:

$$Y' = mX' + b, \text{ with: } Y' = \log(R_0) \text{ and: } X' = \log(A_D),$$

the following values (with standard errors) were found for 8 membranes (see Fig. 5b): $m = -0.96 \pm 0.03$, $b = 2.54 \pm 0.02$, $r = -0.996$. Doing the same calculations with: $Y' = \log(\omega_{\max})$ and: $X' = \log(A_D)$, the results were (see Fig. 5b): $m = 1.46 \pm 0.12$, $b = 4.40 \pm 0.06$. $r = 0.98$.

$\text{Log}(K_\alpha)$ and α failed to show significant correlation with $\log(A_D)$.

Discussion

The 6-parameter model offers a good description of the impedance spectra of enamel, and the values of R_0 and $\omega_{\max}$ calculated using this model are fairly reliable predictors for the ion-permeability of tooth enamel. However, a drawback of this approach, that arises partly because Eqs. (1) and (2) do not obey the Kramers-Kronig relations (see however: [18]) is, that it cannot be related to physical structures and mechanisms and/or chemical processes. The analysis using CPA-elements has the advantage that the occurrence of such an element in an equivalent circuit may be associated with the presence of an inhomogeneous diffusion process.

Enamel membranes have a flow-through system with an isolating support-material (mineral crystallites) and pores whose dimensions approach those of the charge-carriers. The process leading to the observed shape of the complex impedance spectra is the relaxation of the electrolyte within the confinements offered by such a pore-structure. This relaxation may be interpreted as an interaction between the resistance of the electrolyte solution in the pores, that together constitute the "forward" conductance pathways also used by diffusion, and the capacities associated with the "transverse" conduction pathways offered by the double layer that lines the pore-walls and the geometric capacities, that arise because of the physical separation of two confining pores.

So, looking at one pore and its direct environment, a relaxation-time, $\tau_\mu = R_{o,p} \cdot C_{pp}$ is observed. Approximate expressions for $R_{o,p}$, the resistance of the pore-interior and C_{pp}, the (mutual) pore-pore capacity, are derived elsewhere [19, 20]. Due to physiological variations a considerable diversity will be found in the structural parameters that determine $R_{o,p}$ and C_{pp}. So a distribution of relaxation-times (rather than one single relaxation-time) will be observed in the time-domain for a certain specimen of enamel. In this case it can be derived that:

$$\tau_0 = R_0 \cdot C_\alpha \tag{11}$$

where τ_0 indicates the position of the maximum in the distribution, and C_α may be interpreted as the average value of C_{pp}. In the frequency-domain this corresponds with the occurrence of a resistor constant-phase-angle element parallel circuit, which shapes the complex impedance spectrum in a semi-arc, whose center is depressed below the real axis (cf. [5]).

The reciprocal correlation between R_0 and A_D can be elucidated as follows. R_0 is inversely proportional to G_{exp}, the conductivity offered by the ensemble of all conducting pathways (i.e. the pore-system) of a membrane. This conductivity will be proportional to the available transport-volume, i.e. to the porosity of the considered membrane. As shown [19, 20], variations in membrane porosity appear to be the main determinants for explaining the observed range both in conductivity and in permeability (the influence of variations in the average pore-radius and membrane-charge appears to be much smaller). Thus permeability and conductivity are strictly interrelated via the membrane-porosity, which in turn explains the observed reciprocal correlation between R_0 and A_D.

The observed relation between $\omega_{\max}$ and A_D may provisionally be clarified as follows:

Since $\omega_{\max} = 1/\tau_0$, the following relation holds:

$$\omega_{\max} = G_{\text{exp}}/C_\alpha. \tag{12}$$

G_{exp} is proportional to A_D (see above) and C_α showed a slight decrease with increasing values of A_D (m_α, the slope in a plot of $\log(C_\alpha)$ versus $\log(A_D)$ was -0.30 ± 0.06. This means, that the importance of a capacitive conduction mechanism decreases with increasing permeability, a finding that is congruent with vanishing capacities for porosities approaching unity. So, according to Eq. (12), m_ω, the slope in a $\log(\omega_{\max})$ versus $\log(A_D)$ plot, will be $1 - m_\alpha$. i.e. 1.30 ± 0.06, which is not significantly different from the experimental value of m_α (1.46 ± 0.12).

In case the relaxation times of the system are not normally distributed, more complicated equivalent circuits will be necessary. For a membrane with a non-gaussian pore distribution (see Fig. 6a) an electric analogue as drawn in

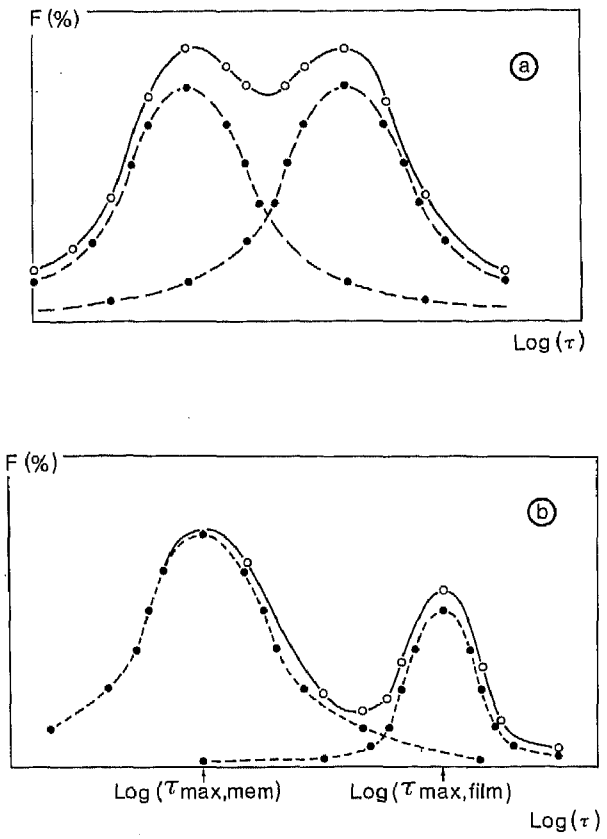

Fig. 6
a) Example of a non-gaussian distribution of relaxation times τ. F denotes the density function. Note: the open and solid dots in this figure refer to simulated data and not to actual measurements.
b) Bimodal distribution-function as expected in the presence of a surface-film (refer to note of Fig. 6a).

Fig. 2b will be found. The parallel connection of Fig. 2b would, on a physical level, translate into a lateral membrane inhomogeneity, i.e. confining regions of pores with different pore radius distributions.

When there is an apolar surface-film on the membrane (cf. [21]), with such properties that the distribution of relaxation times of this film differs strongly from that of the membrane (i.e. $\omega_{max,mem} - \omega_{max,film} > 1$, see Fig. 6b and [17]), an extra RQP will appear in the equivalent circuit, in series with the one that corresponds with the membrane (see Fig. 2c). The Cole-Cole plot that would be measured in this situation is drawn in Fig. 1b. So, the low-frequency deviations found for some enamel specimen (see Results), may be due to the presence of laminar membrane inhomogeneities, which means that inside the membrane there exists a series-connection of layers with differing structure and permeability. This phenomenon was postulated earlier [1] in computer-simulations of the progress of early subsurface enamel lesions and confirmed by scanning the electrochemical conductivity of consecutive surface-enamel layers [22].

Conversely one may conclude that the sufficiency of one RQP-branch for a typical bulk enamel membrane points to a monomodal pore-radius distribution, which contrasts with the results of Moreno and Zahradnik [23], who found a bimodal distribution. This discrepancy may partly be resolved, by arguing that part of the fine-structure revealed by the water-sorption/desorption studies (namely for hydraulic radii smaller than 0.5 to 1.0 nm) will be virtually inaccessible to the permeating species used in the present work. Furthermore, as Dibdin and Poole [24] point out, errors up to 45% may be present in the results of Moreno und Zahradnik [23], due to the assumptions made in calculating the distribution.

The authors would like to thank R. Gorissen for his skilful technical assistance and M. Ouwekerk for his contribution in the analysis of some enamel impedance spectra with the network analysis software implemented at the Solid State Department of the Utrecht Physics Laboratory.

H. Scholberg would like to thank M. Graaf, F. de Groot and F. Pijpers for their inspiring discussions.

Refrences

[1] J. W. E. van Dijk, J. M. P. M. Borggreven, and F. C. M. Driessens, Caries Res. *13*, 169 (1979).
[2] J. M. P. M. Borggreven, J. W. E. van Dijk, and F. C. M. Driessens, Archs. Oral Biol. *22*, 467 (1977).
[3] H. P. F. Scholberg, J. M. P. M. Borggreven, and F. C. M. Driessens, Med. Biol. Eng. Comp. *20*, 578 (1982).
[4] H. P. F. Scholberg, J. M. P. M. Borggreven, and F. C. M. Driessens, Archs. Oral Biol. *29*, 965 (1984).
[5] C. J. F. Boettcher and P. Bordewijk, Theory of electric polarisation, Vol. II, p. 1, Dielectrics in time-dependent fields, second edition, Elsevier Scient. Publ. Corp., Amsterdam 1978.
[6] I. D. Raistrick, C. Ho, Y. W. Hu, and R. A. Huggins, J. Electroanal. Chem. *77*, 319 (1977).
[7] I. D. Raistrick, C. Ho, and R. A. Huggins, J. Electrochem. Soc. *123*, 1469 (1977a).
[8] E. D. Raistrick, C. Ho, and R. A. Huggins, J. Electrochem. Soc. *124*, 871 (1977b).
[9] J. R. Mcdonald and M. K. Brachman, Rev. Mod. Phys. *28*(4), 393 (1956).
[10] R. U. E. 't Lam, J. Schoonman, and G. Blasse, Ber. Bunsenges. Phys. Chem. *85*, 592 (1981).
[11] J. R. McDonald, J. Schoonman, and A. P. Lehnen, J. Electroanal. Chem. *131*, 77 (1982).
[12] K. Levenberg, Quart. Appl. Math. *2*, 164 (1944).
[13] D. W. Marquardt, , J. Soc. Industr. Appl. Math. *11*, 431 (1963).
[14] Y. T. Tsai and D. H. Whitmore, Solid State Ionics *7*, 129 (1982).
[15] R. J. Sheppard, B. P. Jordan, and E. H. Grant, J. Phys. D. (Appl. Phys.) *3*, 1759 (1970).
[16] R. J. Sheppard, J. Phys. D. (Appl. Phys.) *6*, 790 (1973).
[17] M. Kleitz and J. H. Kennedy, Resolution of multicomponent impedance diagrams, in: P. Vashishta, J. N. Mundy, and G. K. Shenoy (eds.), Fast Ion Transport in Solids, p. 185, North-Holland, Amsterdam 1979.
[18] R. L. Van Meirhaeghe, E. C. Dutoit, F. Cardon, and W. P. Gomes, Electrochim. Acta *20*, 995 (1975).
[19] H. P. F. Scholberg and J. M. P. M. Borggreven, A structural interpretation of impedance spectra and radio-isotope diffusion in dental enamel, Ber. Bunsenges. Phys. Chem., accepted for publication.
[20] H. P. F. Scholberg, Permeability of tooth enamel membranes: a study of complex impedance measurements, Thesis, University of Nijmegen 1985.
[21] R. P. Buck, J. Electroanal. Chem. *18*, 363 (1968).
[22] P. M. M. Hoppenbrouwers, H. P. F. Scholberg, and J. M. P. M. Borggreven, J. Dent. Res. *65*, 154 (1986).
[23] E. C. Moreno and R. T. Zahradnik, Archs. Oral Biol. *18*, 1063 (1973).
[24] G. H. Dibdin and D. F. G. Poole, Archs. Oral Biol. *27*, 235 (1982).

(Eingegangen am 18. Oktober 1985, endgültige Fassung am 9. September 1986) E 6113